BULLETIN OF THE POLISH ACADEMY OF SCIENCES
TECHNICAL SCIENCES, Vol. 70(5), 2022, Article number: e141985
DOI: 10.24425/bpasts.2022.141985

ADI-based, conditionally stable schemes for seismic P-wave and elastic wave propagation problems

Marcin ŁOŚ[1], **Pouria BEHNOUDFAR**[2], **Mateusz DOBIJA**[3], **and Maciej PASZYŃSKI**[1]*

[1] AGH University of Science and Technology, Faculty of Computer Science, Electronics and Telecommunications, al. Mickiewicza 30, 30-059 Krakow, Poland
[2] Mineral Resources, Commonwealth Scientific and Industrial Research Organisation (CSIRO), Kensington, Perth, Western Australia
[3] Jagiellonian University, Faculty of Astronomy, Physics and Applied Computer Science, Kraków, Poland

Abstract. The modeling of P-waves has essential applications in seismology. This is because the detection of the P-waves is the first warning sign of the incoming earthquake. Thus, P-wave detection is an important part of an earthquake monitoring system. In this paper, we introduce a linear computational cost simulator for three-dimensional simulations of P-waves. We also generalize our formulations and derivation for elastic wave propagation problems. We use the alternating direction method with isogeometric finite elements to simulate seismic P-wave and elastic propagation problems. We introduce intermediate time steps and separate our differential operator into a summation of the blocks, acting along the particular coordinate axis in the sub-steps. We show that the resulting problem matrix can be represented as a multiplication of three multi-diagonal matrices, each one with B-spline basis functions along the particular axis of the spatial system of coordinates. The resulting system of linear equations can be factorized in linear $\mathcal{O}(N)$ computational cost in every time step of the semi-implicit method. We use our method to simulate P-wave and elastic wave propagation problems. We derive the condition for the stability of seismic waves; namely, we show that the method is stable when $\tau < C\min\{h_x, h_y, h_z\}$, where C is a constant that depends on the PDE problem and also on the degree of splines used for the spatial approximation. We conclude our presentation with numerical results for seismic P-wave and elastic wave propagation problems.

Key words: conditional stability; P-wave propagation problems; elastic wave propagation problems; linear computational cost; time-dependent simulations.

1. INTRODUCTION

The modeling of P-waves has essential application in seismology, as their detection can be used for the prediction of earthquakes [1]. The P-wave detection is a crucial component of the earthquake monitoring system [2]. The seismology simulations are usually performed with the Spectral Finite Element Method [3, 4]. We present a linear computational cost simulator for three-dimensional P-wave simulations. We use an alternating direction method with isogeometric finite elements to simulate P-wave propagation problems. We also generalize our formulations and derivation for elastic wave propagation problems. In our numerical examples, we employ isotropic material. We also show that our method can be extended to the anisotropic case, as it is commonly required in seismology simulations [5].

The isogeometric analysis (IGA) [6] is a modern method for performing finite element method (FEM) simulations with B-splines and NURBS. The IGA-FEM has multiple applications for simulations of time-dependent problems, including wind turbine aerodynamics [7], turbulent flow simulations [8], phase-field and phase-separation simulations [9–12], incompressible hyper-elasticity [13], blood flow simulations [14–17] tumor growth simulations [18, 19], and covid propagation [20]. The main idea of the isogeometric analysis (IGA) [6, 21] is to apply B-splines or NURBS basis functions in finite element simulations. The direction splitting method was used in the past to accelerate finite difference simulation of time-dependent problems [22–24]. The method has been recently "rediscovered" for the isogeometric finite element method. It is employed to speed up non-stationary simulations for elliptic problems [25–28]. The direction splitting schemes deliver a fast inversion method for the spatial discretization, which is obtained by grouping together the one-dimensional B-splines along particular spatial axes, assuming the mesh has a tensor product structure. The method was used for performing fast explicit dynamics simulations [29, 30] expressed as the sequence of isogeometric L2 projections, which can be solved using the direction splitting method. The limitation of the method is the assumption about the tensor product structure of the computational mesh. The two-dimensional version of the direction-splitting algorithm has been employed for second-order hyperbolic initial-boundary value problems [31]. Here we focus on 3D formulation with quadratic B-spline basis functions. There is also a numerical method for viscous and nonviscous wave equations [32]. A similar method applied for the heat transfer problem results in an unconditionally stable time integration scheme [33].

This paper extends this methodology to the seismic P-wave and elastic wave propagation problems by collecting different terms as a sequence of multi-banded inversions. The alternative

*e-mail: paszynsk@agh.edu.pl

Manuscript submitted 2022-03-13, revised 2022-06-07, initially accepted for publication 2022-06-09, published in October 2022.

approaches involve iterative or multi-frontal solvers [34, 35]. Its computational costs vary from $\mathcal{O}(Nk)$ for iterative solvers, where N is the problem size, and k is the number of iterations. This number of iterations is problem-dependent. The upper bound for the cost is $\mathcal{O}(N^2p^3)$ for the multi-frontal solvers, where N is the problem size and p is the B-splines order. In this paper, we propose a direct solver algorithm with linear $\mathcal{O}(N)$ computational cost.

An alternative way of dealing with hyperbolic problems is presented in [36]. The alternative method presented in [36] neglects the higher-order terms in the approximation of $(M_x + \eta K_x) \otimes (M_y + \eta K_y) = M_x \otimes M_y + \eta M_x \otimes K_y + \eta K_x \otimes M_y + \eta^2 K_x \otimes K_y \approx M_x \otimes M_y + \eta M_x \otimes K_y + \eta K_x \otimes M_y$, where we have denoted the one-dimensional mass M_x and stiffness K_x matrices. In our method we do not neglect the higher order terms.

The structure of the paper is the following. In Section 2, we start from the description of the direction splitting for the P-wave propagation, with stability analysis in Section 3 and numerical results for P-wave propagation problems summarized in Section 4. In Section 5, we generalize our formulation for elastic wave propagation problems. In Section 6 we present numerical results for the elastic wave propagation problems, and in Section 7 we discuss a possible extension to the anisotropic case. Finally, we conclude the paper in Section 8.

2. DIRECTION SPLITTING FOR P-WAVE PROPAGATION PROBLEM

We solve first the scalar P-wave equation problem given by

$$\ddot{u} - \Delta u = f \tag{1}$$

with $u(0) = u_0$, and $\dot{u}(0) = v_0$. We employ zero Neumann boundary conditions $\nabla u \cdot n = 0$, where n is the versor normal to the boundary. We discretize time

$$\ddot{u}_{n+1} - \Delta u_{n+1} = f_{n+1} \tag{2}$$

and use Newmark expansion from time step n to $n+1$ [37]

$$u_{n+1} = u_n + \Delta t\, \dot{u}_n + \frac{1}{2}\Delta t^2\, \ddot{u}_{n+1} \tag{3}$$

so that

$$\ddot{u}_{n+1} - \frac{1}{2}\Delta t^2\, \Delta\ddot{u}_{n+1} = \Delta u_n + \Delta t\, \Delta\dot{u}_n + f_{n+1}\,. \tag{4}$$

In these formulas, we have different units for $u[m]$, $\dot{u}[m/s]$, $\ddot{u}[m/s^2]$ and $\Delta u[m/m^2]$. For consistency with the physical interpretation, we can introduce constants equal to 1, with suitable units, so globally the units coincide, e.g. $\ddot{u}[m/s^2] - \Delta u[m/m^2] * 1[m^2/s^2] = f[m/s^2]$. We compute u_n, $\dot{u}_n$ and $\ddot{u}_n$ as three independent quantities. We can update $\dot{u}_n$ according to

$$\dot{u}_{n+1} = \dot{u}_n + \Delta t\, \ddot{u}_{n+1}\,. \tag{5}$$

As for the u_n, using the Taylor expansion (backwards) we get

$$u_n = u_{n+1} - \Delta t\, \dot{u}_{n+1} + \frac{1}{2}\Delta t^2\, \ddot{u}_{n+1} \tag{6}$$

and so

$$u_{n+1} = u_n + \Delta t\, \dot{u}_{n+1} - \frac{1}{2}\Delta t^2\, \ddot{u}_{n+1}\,. \tag{7}$$

The full scheme is thus the following:

$$\begin{cases} \ddot{u}_{n+1} - \dfrac{1}{2}\Delta t^2\, \Delta\ddot{u}_{n+1} = \Delta u_n + \Delta t\, \Delta\dot{u}_n + f_{n+1}\,, \\ \dot{u}_{n+1} = \dot{u}_n + \Delta t\, \ddot{u}_{n+1}\,, \\ u_{n+1} = u_n + \Delta t\, \dot{u}_{n+1} - \dfrac{1}{2}\Delta t^2\, \ddot{u}_{n+1}\,. \end{cases} \tag{8}$$

Both u_{n+1} and $\dot{u}_{n+1}$ can be trivially computed given $\ddot{u}_{n+1}$. For $\ddot{u}$, we split the Laplacian and introduce intermediate time steps:

$$\begin{aligned} \ddot{u}_{n+1/3} - \frac{1}{2}\tau^2\, \partial_{xx}\ddot{u}_{n+1/3} &= \frac{1}{2}\tau^2\, (\partial_{yy}\ddot{u}_n + \partial_{zz}\ddot{u}_n) \\ &\quad + \Delta u_n + \Delta t\, \Delta\dot{u}_n + f_{n+1/3}\,, \\ \ddot{u}_{n+2/3} - \frac{1}{2}\tau^2\, \partial_{yy}\ddot{u}_{n+2/3} &= \frac{1}{2}\tau^2\, \left(\partial_{xx}\ddot{u}_{n+1/3} + \partial_{zz}\ddot{u}_{n+1/3}\right) \\ &\quad + \Delta u_{n+1/3} + \Delta t\, \Delta\dot{u}_{n+1/3} + f_{n+2/3}\,, \\ \ddot{u}_{n+1} - \frac{1}{2}\tau^2\, \partial_{xx}\ddot{u}_{n+1} &= \frac{1}{2}\tau^2\, \left(\partial_{xx}\ddot{u}_{n+2/3} + \partial_{xx}\ddot{u}_{n+2/3}\right) \\ &\quad + \Delta u_{n+2/3} + \Delta t\, \Delta\dot{u}_{n+2/3} + f_{n+1}\,, \end{aligned} \tag{9}$$

where $\tau = \Delta t/3$ and $\dot{u}_{n+k/3}$, $\ddot{u}_{n+k/3}$ are computed according to (8). After multiplying by the test function w and integrating the second derivatives by parts, we obtain

$$\begin{aligned} (\ddot{u}_{n+1/3}, w)_{L^2} + \frac{1}{2}\tau^2 (\partial_x\ddot{u}_{n+1/3}, \partial_x w)_{L^2} &= \\ - \frac{1}{2}\tau^2 (\partial_y\ddot{u}_n, \partial_y w)_{L^2} & \\ - \frac{1}{2}\tau^2 (\partial_z\ddot{u}_n, \partial_z w)_{L^2} & \\ - (\nabla u_n, \nabla w)_{L^2} & \\ - \Delta t\, (\nabla\dot{u}_n, \nabla w)_{L^2} + (f_{n+1/3}, w)_{L^2}\,, & \\ (\ddot{u}_{n+2/3}, w)_{L^2} + \frac{1}{2}\tau^2 (\partial_y\ddot{u}_{n+2/3}, \partial_y w)_{L^2} &= \\ - \frac{1}{2}\tau^2 (\partial_x\ddot{u}_{n+1/3}, \partial_x w)_{L^2} & \\ - \frac{1}{2}\tau^2 (\partial_z\ddot{u}_{n+1/3}, \partial_z w)_{L^2} & \\ - (\nabla u_{n+1/3}, \nabla w)_{L^2} & \\ - \Delta t\, (\nabla\dot{u}_{n+1/3}, \nabla w)_{L^2} + (f_{n+2/3}, w)_{L^2}\,, & \\ (\ddot{u}_{n+1}, w)_{L^2} + \frac{1}{2}\tau^2 (\partial_z\ddot{u}_{n+1}, \partial_z w)_{L^2} &= \\ - \frac{1}{2}\tau^2 (\partial_x\ddot{u}_{n+2/3}, \partial_x w)_{L^2} & \\ - \frac{1}{2}\tau^2 (\partial_y\ddot{u}_{n+2/3}, \partial_y w)_{L^2} & \\ - (\nabla u_{n+2/3}, \nabla w)_{L^2} & \\ - \Delta t\, (\nabla\dot{u}_{n+2/3}, \nabla w)_{L^2} + (f_{n+1}, w)_{L^2}\,. & \end{aligned} \tag{10}$$

Integrating by parts

$$(\partial_{xx}\partial_{tt}u, w) = \partial_{tt}(\partial_{xx}u, w) = \partial_{tt}(\partial_x u, \partial_x w) - \partial_{tt}\int_{\partial\Omega} n_x w \partial_x u \, \mathrm{d}\sigma$$

for all but two of the sides, the n_x component of the normal versor is equal to 0, and on the other two sides, the Neumann boundary condition implies $\partial_x u = 0$. Similar considerations can be applied for ∂_{yy} and ∂_{zz}. We discretize with B-splines basis functions of order p employed in isogeometric analysis. For example, for the first equation we have

$$\ddot{u}_{n+1/3} = \sum_{i,j,k} v_{i,j,k} B^x_{i;p}(x) B^y_{j;p}(y) B^z_{k;p}(z) = \sum_{i,j,k} v_{i,j,k} B_i(x) B_j(y) B_k(z)$$

and $w = B^x_{l;p}(x) B^y_{m;p}(y) B^z_{n;p} = B_l(x) B_m(y) B_n(z)$.

The matrix on the left-hand side

$$A_{ijk,lmn} = (B_{ijk}, B_{lmn})_{L^2} - \frac{\tau^2}{2}(\partial_x B_{ijk}, \partial_x B_{lmn})_{L^2} \tag{11}$$

$$= \int_\Omega \partial_x B_{ijk} B_{lmn} - \frac{\tau^2}{2}\int_\Omega \partial_x B_{ijk} \partial_x B_{lmn} \tag{12}$$

$$= \int_\Omega (B_i B_l)(x)\,(B_j B_m)(y)\,(B_k B_n)(z)\,\mathrm{d}\Omega \tag{13}$$

$$- \frac{\tau^2}{2}\int_\Omega (\partial_x B_i \partial_x B_l)(x)\,(B_j B_m)(y)\,(B_k B_n)(z)\,\mathrm{d}\Omega \tag{14}$$

$$= \left(\int_{\Omega_x} B_i B_l \,\mathrm{d}x\right)\left(\int_{\Omega_y} B_j B_m \,\mathrm{d}y\right)\left(\int_{\Omega_z} B_k B_n \,\mathrm{d}z\right) \tag{15}$$

$$- \frac{\tau^2}{2}\left(\int_{\Omega_x} B_i \partial_x B_l \,\mathrm{d}x\right)\left(\int_{\Omega_y} B_j B_m \,\mathrm{d}y\right)\left(\int_{\Omega_z} B_k B_n \,\mathrm{d}z\right) \tag{16}$$

$$= (M_x^{il} - \frac{\tau^2}{2}K_x^{il}) M_y^{jm} M_z^{kn}, \tag{17}$$

where we have denoted the one-dimensional mass M_x and stiffness K_x matrices. This implies $A = \left(M_x - \frac{\tau^2}{2}K_x\right) \otimes M_y \otimes M_z$. In other words, our system is the Kronecker product of three multi-diagonal matrices with the corresponding structure of one-dimensional B-spline basis functions. The other matrices have the same feature. Such the matrix can be factorized in a linear computational cost [38].

3. STABILITY OF P-WAVE PROPAGATION PROBLEM

To study the stability behavior of the method, we stick to 2D case without loss of generality. The Newmark method, comprised by (8) and (10), can be rewritten in the following way. Following the weak form of (10) for 2D

$$\left(M + \frac{1}{2}\tau^2 K_x \otimes M_y\right)\ddot{u}_{n+\frac{1}{2}} = -\frac{1}{2}\tau^2 M_x \otimes K_y \ddot{u}_n - K u_n - \tau K \dot{u}_n + f_{n+\frac{1}{2}}, \tag{18}$$

where $M = M_x \otimes M_y$ is the 2D mass matrix, and $K = K_x \otimes K_y$ is the 2D stiffness matrix.

$$\begin{bmatrix} u^{n+\frac{1}{2}} \\ \dot{u}^{n+\frac{1}{2}} \\ \ddot{u}^{n+\frac{1}{2}} \end{bmatrix} = \begin{bmatrix} I - \frac{1}{2}\gamma\tau^2 K & \tau(I - \frac{1}{2}\gamma\tau^2 K) & \frac{1}{2}\tau^2\Psi \\ -\gamma\tau K & I - \gamma\tau^2 K & \tau\Psi \\ -\gamma K & -\gamma\tau K & \Psi \end{bmatrix} \begin{bmatrix} u^n \\ \dot{u}^n \\ \ddot{u}^n \end{bmatrix} + \begin{bmatrix} F_{n+\frac{1}{2}} \end{bmatrix}, \tag{19}$$

where we have

$$I = I_x \otimes I_y,$$
$$\gamma = (M_x + \frac{1}{2}\tau^2 K_x)^{-1} \otimes M_y^{-1},$$
$$\Psi = -\frac{1}{2}\tau^2 \gamma (M_x \otimes K_y).$$

We ignore the forcing terms, whereas the generality of the stability proof is still guaranteed. In the next step, we follow an approach to obtain the spectral decomposition of stiffness matrix K_η with respect to M_η

$$K_\eta v_\eta = \lambda_\eta M_\eta v_\eta, \tag{20}$$

where η denotes the dimension as $\eta = x, y$.

Since the amplification matrix to obtain unknowns at $t_{n+1/2}$ from given data at time t_n is the same as the system providing solution at t_{n+1} from data at $t_{n+1/2}$, with roles of x and y exchanged, we only consider the system (19) to study the behaviour of marching from time $t_{n+1/2}$ to t_{n+1}. This approach is valid as showing the stability of the solution at the next time step is important.

We set the eigenvalues λ in a diagonal matrix D_η and the eigenvectors v in the columns of a matrix P_η. It should also be noted that the j-th column of P_η is associated with the eigenvalue $\lambda_j = D_{jj}$. Hence, we have

$$K_\eta = M_\eta P_\eta D_\eta P_\eta^{-1}. \tag{21}$$

Using (21) and the fact that $I_\eta = P_\eta I_\eta P_\eta^{-1}$, we calculate

$$\gamma = \left(M_x + \zeta M_x P_x D_x P_x^{-1}\right)^{-1} \otimes M_y^{-1} = \left(M_x (I_x + \frac{1}{2}P_x D_x P_x^{-1})\right)^{-1} \otimes M_y^{-1} = \left(P_x (I_x + \zeta D_x)^{-1} P_x^{-1} M_x^{-1}\right) \otimes M_y^{-1}. \tag{22}$$

where $\zeta = \frac{1}{2}\tau^2$. Finally, we obtain:

$$\begin{aligned}\gamma K &= \left\{\left(P_x E_x P_x^{-1} M_x^{-1}\right)\otimes M_y^{-1}\right\} \\ &\quad \left\{M_x \otimes M_y P_y D_y P_y^{-1} + M_x P_x D_x P_x^{-1}\otimes M_y\right\} \\ &= (P_x\otimes P_y)\Big(E_x\otimes D_y + E_x D_x \otimes I_y\Big)(P_x^{-1}\otimes P_y^{-1}), \end{aligned} \tag{23}$$

$$\begin{aligned}\gamma\Psi &= \left\{\left(P_x E_x P_x^{-1} M_x^{-1}\right)\otimes M_y^{-1}\right\}\left\{M_x\otimes M_y P_y D_y P_y^{-1}\right\} \\ &= (P_x\otimes P_y)\Big(E_x\otimes D_y\Big)(P_x^{-1}\otimes P_y^{-1}), \end{aligned} \tag{24}$$

where $E_x = \Big(I_x + \zeta D_x\Big)^{-1}$.

Then, it is possible to rewrite the amplification matrix in (19) as follows (where we have broken the rows in the amplification matrix to fit into the two-column format of the paper)

$$\Xi = \begin{bmatrix} P_x\otimes P_y\left(I-\frac{1}{2}\tau^2 G\right)P_x^{-1}\otimes P_y^{-1} & P_x\otimes P_y\left(\tau I-\frac{1}{2}\tau^3 G\right)P_x^{-1}\otimes P_y^{-1}\cdots \\ & \cdots P_x\otimes P_y\left(-\frac{1}{4}\tau^4 H\right)P_x^{-1}\otimes P_y^{-1} \\ P_x\otimes P_y(-\tau G)P_x^{-1}\otimes P_y^{-1} & P_x\otimes P_y(I-\tau^2 G)P_x^{-1}\otimes P_y^{-1}\cdots \\ & \cdots P_x\otimes P_y\left(-\frac{1}{2}\tau^3 H\right)P_x^{-1}\otimes P_y^{-1} \\ P_x\otimes P_y(-G)P_x^{-1}\otimes P_y^{-1} & P_x\otimes P_y(-G)P_x^{-1}\otimes P_y^{-1}\cdots \\ & \cdots P_x\otimes P_y\left(-\frac{1}{2}\tau^2 H\right)P_x^{-1}\otimes P_y^{-1}\end{bmatrix}$$

$$= \begin{bmatrix} P_x\otimes P_y & 0 & 0 \\ 0 & P_x\otimes P_y & 0 \\ 0 & 0 & P_x\otimes P_y\end{bmatrix}$$

$$\begin{bmatrix} I_x\otimes I_y-\frac{1}{2}\tau^2 G & \tau(I_x\otimes I_y)-\frac{1}{2}\tau^3 G & -\frac{1}{4}\tau^4 H \\ -\tau G & I_x\otimes I_y-\tau^2 G & -\frac{1}{2}\tau^3 H \\ -G & -\tau G & -\frac{1}{2}\tau^2 H\end{bmatrix}$$

$$\begin{bmatrix} P_x^{-1}\otimes P_y^{-1} & 0 & 0 \\ 0 & P_x^{-1}\otimes P_y^{-1} & 0 \\ 0 & 0 & P_x^{-1}\otimes P_y^{-1}\end{bmatrix}. \tag{25}$$

Here, G and H denote $[E_x\otimes D_y + E_x D_x\otimes I_y]$ and $[E_x\otimes D_y]$, respectively. Therefore, our solution will be

$$\begin{bmatrix} u^{n+\frac{1}{2}} \\ \dot{u}^{n+\frac{1}{2}} \\ \ddot{u}^{n+\frac{1}{2}}\end{bmatrix} = \begin{bmatrix} P_x\otimes P_y & 0 & 0 \\ 0 & P_x\otimes P_y & 0 \\ 0 & 0 & P_x\otimes P_y\end{bmatrix}$$

$$\begin{bmatrix} I_x\otimes I_y-\frac{1}{2}\tau^2 G & \tau(I_x\otimes I_y)-\frac{1}{2}\tau^3 G & -\frac{1}{4}\tau^4 H \\ -\tau G & I_x\otimes I_y-\tau^2 G & -\frac{1}{2}\tau^3 H \\ -G & -\tau G & -\frac{1}{2}\tau^2 H\end{bmatrix}^n$$

$$\begin{bmatrix} P_x^{-1}\otimes P_y^{-1} & 0 & 0 \\ 0 & P_x^{-1}\otimes P_y^{-1} & 0 \\ 0 & 0 & P_x^{-1}\otimes P_y^{-1}\end{bmatrix}\begin{bmatrix} u^0 \\ \dot{u}^0 \\ \ddot{u}^0\end{bmatrix}. \tag{26}$$

We denote the matrix raised to power n by $\tilde{\Xi}$. The spectral radius of this matrix should be bounded by one to claim that the solution is stable. The eigenvalues of the amplification matrix are the solutions of:

$$\det(\tilde{\Xi} - \lambda I) = 0, \tag{27}$$

where

$$\tilde{\Xi} = \begin{bmatrix}\Xi_{11} & \Xi_{12} & \Xi_{13} \\ \Xi_{21} & \Xi_{22} & \Xi_{23} \\ \Xi_{31} & \Xi_{32} & \Xi_{33}\end{bmatrix} = \begin{bmatrix} I_x\otimes I_y-\frac{1}{2}\tau^2 G & \tau(I_x\otimes I_y)-\frac{1}{2}\tau^3 G & -\frac{1}{4}\tau^4 H \\ -\tau G & I_x\otimes I_y-\tau^2 G & -\frac{1}{2}\tau^3 H \\ -G & -\tau G & -\frac{1}{2}\tau^2 H\end{bmatrix}. \tag{28}$$

$\tilde{\Xi}$ is a 3×3 block matrix. Equation (28) is defined for a three-by-three amplification matrix, where the entries of this matrix are combinations of mass, stiffness, and identity matrices, defining the G and H matrices. These G and H matrices are diagonal. We need to show that magnitude of eigenvalues of the amplification matrix is less than 1 (the spectral radius of the amplification matrix is less than 1). The $\tilde{\Xi}$ is a block three-by-three matrix, and its nine sub-matrices are diagonal matrices. It is possible to permute the $\tilde{\Xi}$ matrix in such a way that it is block-diagonal with three by three block matrices Q_k. There are no interactions between these block matrices on the diagonal. Each block matrix Q_k has the same structure as (28), with G and H replaced by corresponding diagonal elements G_{kk} of G and H_{kk} of H,

$$Q_k = \begin{bmatrix} 1-\frac{1}{2}\tau^2 G_{kk} & \tau-\frac{1}{2}\tau^3 G_{kk} & -\frac{1}{4}\tau^4 H_{kk} \\ -\tau G_{kk} & 1-\tau^2 G_{kk} & -\frac{1}{2}\tau^3 H_{kk} \\ -G_{kk} & -\tau G_{kk} & -\frac{1}{2}\tau^2 H_{kk}\end{bmatrix}. \tag{29}$$

The eigenvalues of the amplification matrix are the roots of the characteristic polynomial. The characteristic polynomial of the matrix $\tilde{\Xi}$ is the product of the characteristic polynomials of Q_k,

$$\det\left(\tilde{\Xi} - \lambda I\right) = \prod_k \det\left(Q_k - \lambda I\right), \tag{30}$$

where

$$\begin{aligned}\det(Q_k - \lambda I) &= H_{kk}\tau^2\left(\lambda - \frac{1}{2}\right) + \frac{1}{2}\tau^2 G_{kk}\lambda^2 \\ &\quad - \frac{3}{2}\tau^2 G_{kk}\lambda - \frac{1}{2}\tau^2 H_{kk}\lambda^2 - \lambda + 2\lambda^2 - \lambda^3. \end{aligned} \tag{31}$$

By denoting $\tilde{\lambda}_x^i$ and $\tilde{\lambda}_y^i$ the i-th diagonal entry of D_x and D_y, where $k = (k_x, k_y)$, the diagonal entries G_{kk} of matrices G and H_{kk} of H are given by

$$G_{kk} = \frac{\tilde{\lambda}_x^{k_x} + \tilde{\lambda}_y^{k_y}}{1+\zeta\tilde{\lambda}_x^{k_x}}, \qquad H_{kk} = \frac{\tilde{\lambda}_x^{k_x}}{1+\zeta\tilde{\lambda}_x^{k_x}}. \tag{32}$$

To ensure the stability we require the modules of the roots of (31) to be less than 1. Using $\alpha = G_{kk}\tau^2$, $\beta = H_{kk}\tau^2$, the

characteristic polynomian can be rewritten as

$$\begin{aligned}-\det(Q_k-\lambda I) &= P(\lambda)\\ &= \lambda^3+\left(-2+\frac{3}{2}\alpha+\frac{1}{2}\beta\right)\lambda^2\\ &+\left(1-\frac{1}{2}\alpha-\beta\right)\lambda+\frac{1}{2}\beta. \end{aligned} \tag{33}$$

Now, we show that if $\alpha,\beta<\frac{1}{2}$ then the scheme is stable. The discriminant of above cubic polynomial is

$$\begin{aligned}\Delta=\frac{\alpha}{16}&\left(9\alpha^3+172\alpha\beta-96\beta-64+100\alpha\right.\\ &\left.-66\alpha^2\beta-52\alpha^2-47\alpha\beta^2-48\beta^2\right). \end{aligned} \tag{34}$$

It is easy to show that this discriminant is negative $\Delta<0$, thus, the charactersitic polynomial has one real and a pair of conjugate complex roots:

$$z_0 \text{ (real root)}, \quad z_1=\delta+i\sigma, z_2=\delta+i\sigma \text{ (complex roots)}. \tag{35}$$

Let $\kappa^2=z_1z_2=|z_1|^2=|z_2|^2=\delta^2+\sigma^2$. Using the Vieté formula, we get

$$\begin{aligned} z_0\kappa^2&=-\frac{1}{2}\beta,\\ z_0+2\sigma&=2-\frac{3}{2}\alpha-\frac{1}{2}\beta,\\ z\delta z_0+\kappa^2&=1-\frac{1}{2}\alpha-\beta. \end{aligned} \tag{36}$$

In particular, from the first equation we can read that $z_0<0$. We show now that $\kappa^2<1$. Since $\alpha>\beta$, we can write $\alpha=\beta+\xi$, where $\xi>0$, which leads to

$$\begin{aligned} z_0+2\delta&=2-2\beta-\frac{3}{2}\xi,\\ 2\delta z_0+\kappa^2&=1-\frac{3}{2}\beta-\frac{1}{2}\xi. \end{aligned} \tag{37}$$

Using $\beta=-2z_0\kappa^2$ from (36), we get

$$\begin{aligned} z_0+2\delta&=2+4z_0\kappa^2-\frac{3}{2}\xi,\\ 2\delta z_0+\kappa^2&=1+3z_0\kappa^2-\frac{1}{2}\xi. \end{aligned} \tag{38}$$

We compute δ from the first equation of (38), and we substitute it to the second equation. We have

$$\begin{aligned}\kappa^2\left(1+z_0^2-3z_0\right)&=1+z_0^2-2z_0-\underbrace{\frac{1}{2}\xi(1-3z_0)}_{>0}\\ &\le 1+z_0^2+2z_0\\ &<1+4z_0^2-3z_0 \end{aligned} \tag{39}$$

since $z_0<0$, so $\kappa^2<1$.

What remains to show is that $z_0>-1$. Using the second equation of (36), we have $z_0=2(1-\delta)-\frac{3}{2}\alpha-\frac{1}{2}\beta$. Since $\delta\le\kappa<1$ we have $z_0\ge-\frac{3}{2}\alpha-\frac{1}{2}\beta>\frac{3}{2}\frac{1}{2}-\frac{1}{2}\frac{1}{2}=-1$. Thus, $z_0>-1$, which completes the proof.

Now, we demonstrate that condition $\alpha,\beta<\frac{1}{2}$ is satisfied provided that

$$\max\{\lambda_x^{k_x},\lambda_y^{k_y}\}\tau^2<\frac{1}{4}. \tag{40}$$

We have

$$\alpha=\frac{\tilde{\lambda}_x^{k_x}+\tilde{\lambda}_y^{k_y}}{1+\frac{1}{2}\tau^2\tilde{\lambda}_x^{k_x}}\tau^2\le\frac{\frac{1}{4}+\frac{1}{4}}{1+\frac{1}{2}\cdot 0}=\frac{1}{2} \tag{41}$$

and $\beta<\alpha<\frac{1}{2}$.

We have $\lambda_x^{k_x}\le\hat{C}h_x^{-2}$ and $\lambda_y^{k_y}\le\hat{C}h_x^{-2}$, for some constant $\hat{C}$ that depends on the problem and the degree of splines. This implies the following stability condition

$$\tau\le C\min\{h_x,h_y\}, \tag{42}$$

with $C=\frac{1}{2\sqrt{\hat{C}}}$.

4. NUMERICAL RESULTS FOR P-WAVE PROPAGATION PROBLEMS

The P-wave simulations using alternating-directions solver have been implemented in IGA-ADI software [29]. We test our algorithm in a scalar P-wave propagation problem over a three-dimensional mesh with $32\times32\times32$ elements. We employ quadratic B-splines. We model a three-dimensional cube, and a short impulse directed towards the origin, applied at the opposite corner of the cube. The applied force is given by

$$\mathbf{F}(\mathbf{x},t)=-\phi(t/t_0)r(\mathbf{x})\,\mathbf{p}, \tag{43}$$

$$\mathbf{p}=(1,1,1), \tag{44}$$

$$t_0=0.02, \tag{45}$$

$$\phi(t)=\begin{cases}t^2(1-t)^2 & \text{if } t\in(0,1),\\ 0 & \text{otherwise,}\end{cases} \tag{46}$$

$$r(\mathbf{x})=10\exp\left(-10\,\|\mathbf{x}-\mathbf{p}\|^2\right). \tag{47}$$

Here $u_0=0$ and $v_0=0$. For our semi-implicit scheme with a time step size 10^{-2}, the simulation is stable. The mesh size is $32\times32\times32$ so $h_x=h_y=h_z=1/32=0.03$ and the time step size is $\Delta t=0.01$. If we increase the time step size to 0.1, the simulation explodes, as presented in Fig. 1 (the kinetic, potential, and total energy blow to infinity). The explicit method requires the time step not larger than 10^{-4}. Using time step size 10^{-3} for explicit dynamics simulation also results in a blowup of the solution.

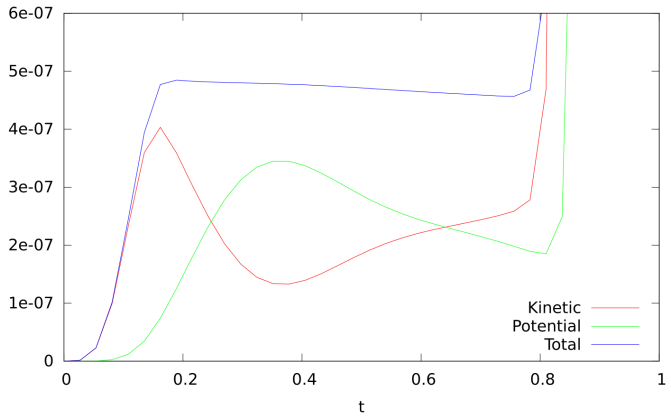

Fig. 1. The kinetic, potential and total energy through the simulation of P-wave propagations with time step 0.1

Moreover, both explicit method with the time step 10^{-4} and the semi-implicit method with the time step 10^{-2} provide identical results, compare the configurations after forty-time steps of the implicit method and four thousand time steps of the explicit method as presented in Fig. 2.

Let us investigate the order of the time integration scheme for the P-waves propagation problem experimentally. These experiments are summarized in Fig. 3. The horizontal axis denotes the time step sizes for different simulation runs, and the vertical axis denotes the L2 and H1 norm computed for the reference solution obtained using the smaller time step. For the P-wave propagation problem, the time integration scheme has an order equal to one. The relation between the accuracy and cost when increasing the mesh size h or B-splines order p follows the analysis discussed in [21].

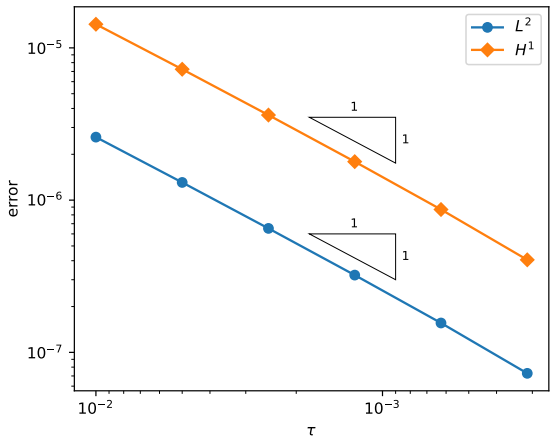

Fig. 3. The order of the time integration scheme for the P-wave propagation problem. Time steps $\Delta t = t_0 = 0.01 = 10^{-2}$, $t_0/2 = 0.005$, $t_0/4 = 0.0025$, $t_0/8 = 0.00125$, $t_0/16 = 0.000625$, $t_0/32 = 0.000312 = 3.12 * 10^{-4}$. The L2 and H1 norms are evaluated from 80 time steps of the simulation and compared against the most accurate simulations with smallest time step $t_0/256$

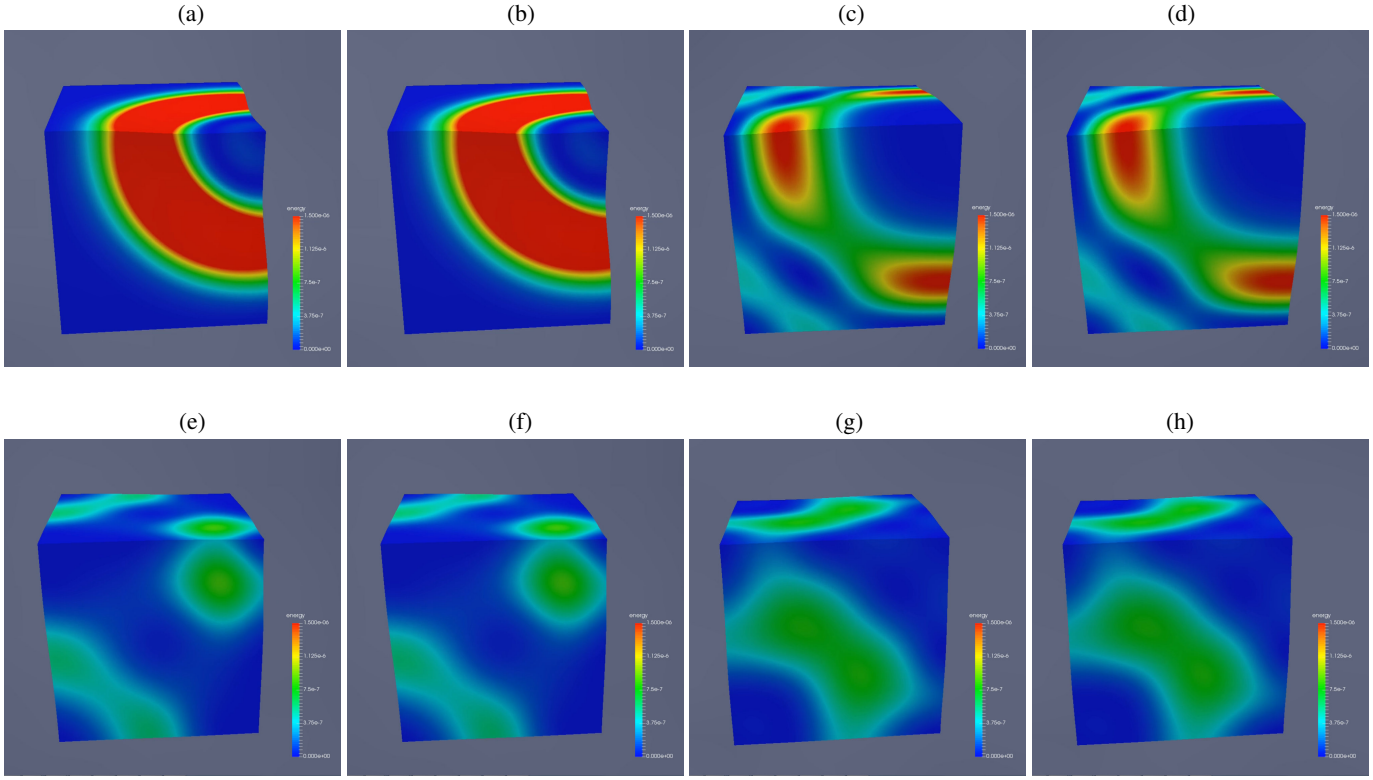

Fig. 2. Comparison of explicit and implicit dynamics for seismic P-wave propagation: (a) snapshot from explicit simulation after 1000 time steps; (b) snapshot from semi-implicit simulation after ten-time steps; (c) snapshot from explicit simulation after 2000 time steps; (d) snapshot from semi-implicit simulation after 20-time steps; (e) snapshot from explicit simulation after 3000-time steps; (f) snapshot from semi-implicit simulation after 30-time steps; (g) snapshot from explicit simulation after 4000-time steps; (h) napshot from semi-implicit simulation after 40-time steps

5. DIRECTION SPLITTING FOR ELASTIC WAVE PROPAGATION

In this section we derive the formulation for elastic wave propagation problem with zero traction boundary conditions

$$\begin{cases} \rho\,\partial_{tt}\mathbf{u} = \nabla\cdot\boldsymbol{\sigma}+\mathbf{F} & \text{on } \Omega\times[0,T],\\ \boldsymbol{u}(x,0) = u_0(x) & \text{for } x\in\Omega,\\ \partial_t\boldsymbol{u}(x,0) = v_0(x) & \text{for } x\in\Omega,\\ \boldsymbol{\sigma}\hat{\mathbf{n}} = 0 & \text{on } \partial\Omega, \end{cases} \tag{48}$$

where $\Omega=[0,1]^3$ is a unit cube, $\mathbf{u}$ is a three-dimensional displacement vector to be calculated, ρ is material density, $\mathbf{F}$ is the applied external force, and $\boldsymbol{\sigma}$ is the Cauchy stress tensor, given by

$$\sigma_{ij} = c_{ijkl}\varepsilon_{lk}\,, \qquad \varepsilon_{ij} = \frac{1}{2}\left(\partial_j u_i + \partial_i u_j\right) \tag{49}$$

and $\mathbf{c}$ is the elasticity tensor. To derive the alternating direction solver for the linear cost calculation, we transform the above second-order system into six first-order equations by introducing an additional vector variable $\mathbf{v}=\partial_t\mathbf{u}$:

$$\begin{cases} \partial_t\mathbf{u} = \mathbf{v}\,,\\ \rho\,\partial_t\mathbf{v} = \nabla\cdot\boldsymbol{\sigma}+\mathbf{F}\,. \end{cases} \tag{50}$$

We assume an isotropic elastic material, and thus the elastic response is fully described by two Lame parameters,

$$\boldsymbol{\sigma} = 2\mu\boldsymbol{\varepsilon}+\lambda\,\mathrm{tr}\,\boldsymbol{\varepsilon}\,I \tag{51}$$

thus

$$\nabla\cdot\boldsymbol{\sigma} = 2\mu(\nabla\cdot\boldsymbol{\varepsilon})+\lambda\,\nabla\,\mathrm{tr}\,\boldsymbol{\varepsilon}\,. \tag{52}$$

Furthermore,

$$\nabla\cdot\boldsymbol{\varepsilon} = \frac{1}{2}\begin{pmatrix} 2\partial_{xx}u_x & +\partial_{yy}u_x+\partial_{yx}u_y & +\partial_{zz}u_x+\partial_{zx}u_z\\ \partial_{xx}u_y+\partial_{xy}u_x & +2\partial_{yy}u_y & +\partial_{zz}u_y+\partial_{zy}u_z\\ \partial_{xx}u_z+\partial_{xz}u_x & +\partial_{yy}u_z+\partial_{yz}u_y & +2\partial_{zz}u_z \end{pmatrix} \tag{53}$$

and

$$\nabla\,\mathrm{tr}\,\boldsymbol{\varepsilon} = \begin{pmatrix} \partial_{xx}u_x+\partial_{xy}u_y+\partial_{xz}u_z\\ \partial_{yx}u_x+\partial_{yy}u_y+\partial_{yz}u_z\\ \partial_{zx}u_x+\partial_{zy}u_y+\partial_{zz}u_z \end{pmatrix}. \tag{54}$$

We split every time-step into three sub-steps

$$\begin{cases} \mathbf{u}^{(t+\frac{1}{3})} = \mathbf{u}^{(t)}+\dfrac{\tau}{3}\mathbf{v}^{(t)},\\ \rho\mathbf{v}^{(t+\frac{1}{3})} = \rho\mathbf{v}^{(t)}+\dfrac{\tau}{3}\left(\nabla\cdot\boldsymbol{\sigma}^{(t+\frac{1}{3})}+\mathbf{F}\right), \end{cases} \tag{55}$$

$$\begin{cases} \mathbf{u}^{(t+\frac{2}{3})} = \mathbf{u}^{(t+\frac{1}{3})}+\dfrac{\tau}{3}\mathbf{v}^{(t+\frac{1}{3})},\\ \rho\mathbf{v}^{(t+\frac{2}{3})} = \rho\mathbf{v}^{(t+\frac{1}{3})}+\dfrac{\tau}{3}\left(\nabla\cdot\boldsymbol{\sigma}^{(t+\frac{2}{3})}+\mathbf{F}\right), \end{cases} \tag{56}$$

$$\begin{cases} \mathbf{u}^{(t+1)} = \mathbf{u}^{(t+\frac{2}{3})}+\dfrac{\tau}{3}\mathbf{v}^{(t+\frac{2}{3})},\\ \rho\mathbf{v}^{(t+1)} = \rho\mathbf{v}^{(t+\frac{2}{3})}+\dfrac{\tau}{3}\left(\nabla\cdot\boldsymbol{\sigma}^{(t+1)}+\mathbf{F}\right) \end{cases} \tag{57}$$

and $\boldsymbol{\sigma}^{(t+\frac{k}{3})}$ are constructed using

$$\mathbf{u} = \mathbf{u}^{(t+\frac{k-1}{3})}+\frac{\tau}{3}\,\mathbf{v}^{(t+\frac{k-1}{3})}$$

in most places, except when u_i appears inside i-th component of $\nabla\cdot\boldsymbol{\sigma}$ under a double derivative with respect to x ($k=1$), y ($k=2$) or z ($k=3$). These cases are marked in equations (53) and (54) with red, magenta, and blue color, respectively. We separate the operator into its diagonal part and its off-diagonal part, treat the diagonal part implicitly, and treat the rest explicitly. After transferring all terms with values to be computed to the left-hand side, the left-hand sides of the sub-diagonal equations have the following form:

$$\begin{cases} \rho\,v_x^{(t+\frac{1}{3})}-\dfrac{\tau}{3}(\lambda+2\mu)\,\partial_{xx}v_x^{(t+\frac{1}{3})}\\ \rho\,v_y^{(t+\frac{1}{3})}-\dfrac{\tau}{3}\mu\,\partial_{xx}v_y^{(t+\frac{1}{3})}\\ \rho\,v_z^{(t+\frac{1}{3})}-\dfrac{\tau}{3}\mu\,\partial_{xx}v_z^{(t+\frac{1}{3})} \end{cases} \tag{58}$$

$$\begin{cases} \rho\,v_x^{(t+\frac{2}{3})}-\dfrac{\tau}{3}\mu\,\partial_{yy}v_x^{(t+\frac{2}{3})}\\ \rho\,v_y^{(t+\frac{2}{3})}-\dfrac{\tau}{3}(\lambda+2\mu)\,\partial_{yy}v_y^{(t+\frac{2}{3})}\\ \rho\,v_z^{(t+\frac{2}{3})}-\dfrac{\tau}{3}\mu\,\partial_{yy}v_z^{(t+\frac{2}{3})} \end{cases} \tag{59}$$

$$\begin{cases} \rho\,v_x^{(t+1)}-\dfrac{\tau}{3}\mu\,\partial_{zz}v_x^{(t+1)}\\ \rho\,v_y^{(t+1)}-\dfrac{\tau}{3}\mu\,\partial_{zz}v_y^{(t+1)}\\ \rho\,v_z^{(t+1)}-\dfrac{\tau}{3}(\lambda+2\mu)\,\partial_{zz}v_z^{(t+1)} \end{cases} \tag{60}$$

Each of the resulting sub-step has the following three terms:

$$\rho v_x-\frac{\tau}{3}C_x\frac{\partial^2 v_x}{\partial x^2} = F_x\,, \tag{61}$$

$$\rho v_y-\frac{\tau}{3}C_y\frac{\partial_y^2 v}{\partial y^2} = F_y\,, \tag{62}$$

$$\rho v_z-\frac{\tau}{3}C_z\frac{\partial^2 v_z}{\partial z^2} = F_z\,. \tag{63}$$

Let us focus on the first equation and derive the weak formulation. We can derive the weak form, by taking the L2 scalar product with test function

$$\rho(v_x,w)+\frac{\tau}{3}C_x\left(\frac{\partial v_x}{\partial x_i}\frac{\partial w}{\partial x_i}\right) = (F,w). \tag{64}$$

We discretize with B-splines $v_x=\sum_{i,j,k} v_{i,j,k}B^x_{i;p}(x)B^y_{j;p}(y)B^z_{k;p}(z)$ and $w=B^x_{l;p}(x)B^y_{m;p}(y)B^z_{n;p}$.

The matrix on the left-hand side

$$A_{ijk,lmn} = \rho(B_{ijk}, B_{lmn})_{L^2} + \frac{\tau}{3} C_x (\partial_x B_{ijk}, \partial_x B_{lmn})_{L^2} \tag{65}$$

$$= \rho \int_\Omega \partial_x B_{ijk} B_{lmn} + \frac{\tau}{3} C_x \int_\Omega \partial_x B_{ijk} \partial_x B_{lmn} \tag{66}$$

$$= \rho \int_\Omega (B_i B_l)(x)\,(B_j B_m)(y)\,(B_k B_n)(z)\,\mathrm{d}\Omega \tag{67}$$

$$+ \frac{\tau}{3} C_x \int_\Omega (\partial_x B_i \partial_x B_l)(x)\,(B_j B_m)(y)\,(B_k B_n)(z)\,\mathrm{d}\Omega \tag{68}$$

$$= \rho \left(\int_{\Omega_x} B_i B_l \,\mathrm{d}x \right) \left(\int_{\Omega_y} B_j B_m \,\mathrm{d}y \right) \left(\int_{\Omega_z} B_k B_n \,\mathrm{d}z \right) \tag{69}$$

$$+ \frac{\tau}{3} C_x \left(\int_{\Omega_x} B_i \partial_x B_l \,\mathrm{d}x \right) \left(\int_{\Omega_y} B_j B_m \,\mathrm{d}y \right) \left(\int_{\Omega_z} B_k B_n \,\mathrm{d}z \right) \tag{70}$$

$$= (\rho M^x_{il} + \frac{\tau}{3} C_x K^x_{il}) \otimes M^y_{jm} \otimes M^z_{kn}, \tag{71}$$

where we have denoted the one-dimensional mass M^x and stiffness K^x matrices. In other words, our system is the Kronecker product of three multidiagonal matrices with the corresponding structure of one-dimensional B-spline basis functions. The remaining matrices have the same structure. Such a matrix can be factorized in a linear computational cost [38].

6. NUMERICAL RESULTS FOR ELASTIC WAVE PROPAGATION PROBLEMS

The elastic wave propagation simulations using alternating-directions solver have been implemented in IGA-ADI software [29]. We test our algorithm on a linear elasticity problem over a three-dimensional mesh with $32 \times 32 \times 32$ elements. We also employ quadratic B-splines. We model a three-dimensional cube and a short impulse as in the P-wave simulations, with the same initial conditions. We employ $h_x = h_y = h_z = \frac{1}{32} = 0.03125$. We select $\tau = 10^{-2} = 0.01$.

The explicit method requires the time step not larger than 10^{-4}. Time step size 10^{-3} or larger results in a blow-up of the simulation. Moreover, both the explicit method with the time step 10^{-4} and the semi-implicit method with the time step 10^{-2} provide visually identical results, compare the configurations after forty-time steps of the implicit method and four thousand time steps of the explicit method as presented in Fig. 4.

Let us investigate experimentally the order of the time integration scheme resulting from the direction splitting algorithm. We have executed a sequence of numerical simulations with different time step sizes to propagate elastic waves. These experiments are summarized in Fig. 5. The horizontal axis denotes the time step sizes utilized in the different simulations.

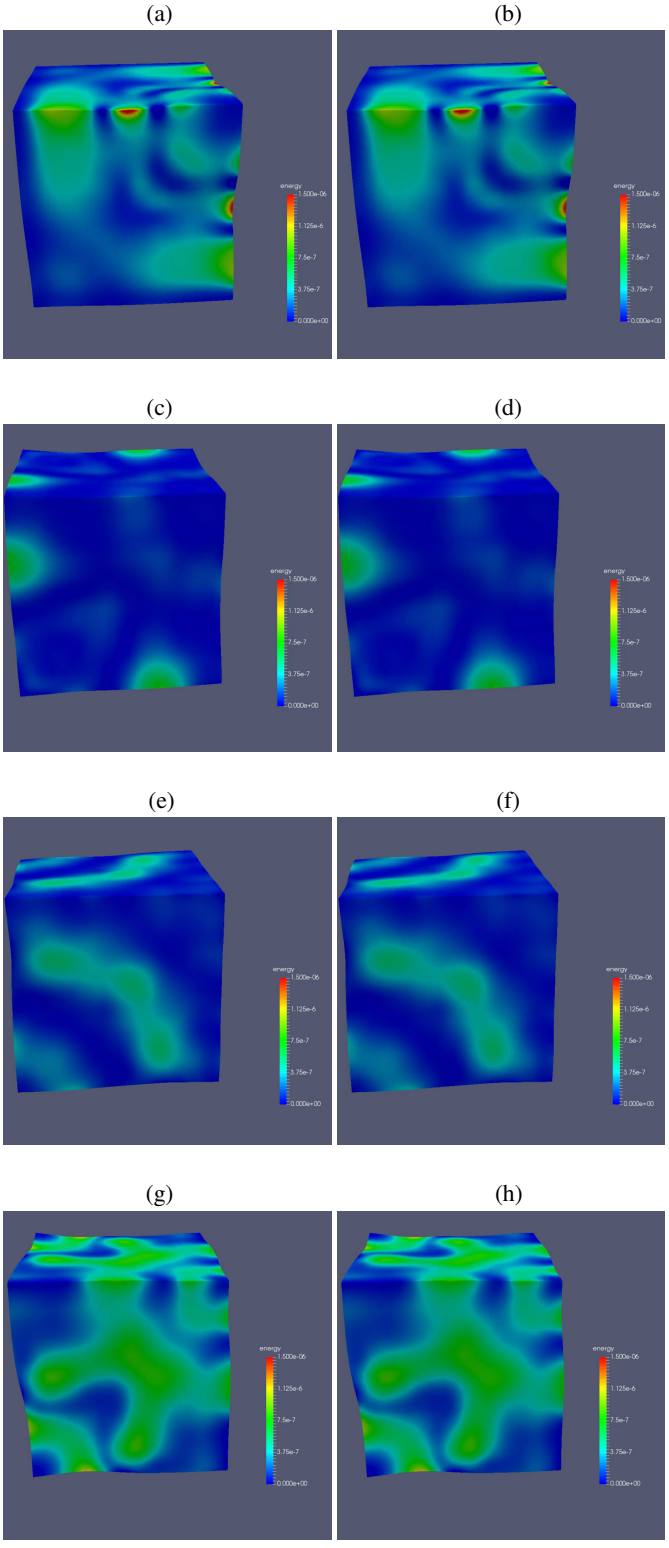

Fig. 4. Comparison of explicit and implicit dynamics for elastic wave propagation: (a) snapshot from explicit simulation after 1000 time steps; (b) snapshot from semi-implicit simulation after ten-time steps; (c) snapshot from explicit simulation after 2000 time steps; (d) snapshot from semi-implicit simulation after 20-time steps; (e) snapshot from explicit simulation after 3000-time steps; (f) snapshot from semi-implicit simulation after 30-time steps; (g) snapshot from explicit simulation after 4000-time steps; (h) snapshot from semi-implicit simulation after 40-time steps

The vertical axis denotes the L2 and H1 norm computed for the reference simulation with the smaller time step. We conclude that our time integration schemes have an order equal to one if we measure the L2 or H1 norms error. On the other hand, increasing p and h follows standard analysis of approximability and accuracy of higher-order B-splines, discussed in [21].

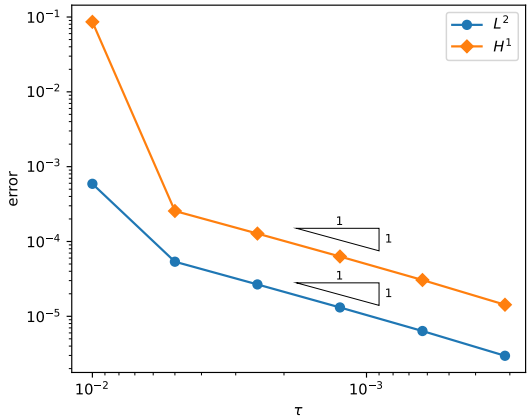

Fig. 5. The order of the time integration scheme for the elastic waves propagation problem. Time steps $\Delta t = t_0 = 0.01 = 10^{-2}$, $t_0/2 = 0.005$, $t_0/4 = 0.0025$, $t_0/8 = 0.00125$, $t_0/16 = 0.000625$, $t_0/32 = 0.000312 = 3.12 \cdot 10^{-4}$. The L2 and H1 norms are evaluated from 80 time steps of the simulation and compared against the most accurate simlations with smallest time step $t_0/256$

7. GENERALIZATION OF THE ELASTIC WAVE PROPAGATION PROBLEM INTO ANISOTROPIC MATERALS

This time, for the elastic wave propagation problem with zero traction boundary conditions

$$\begin{cases} \rho\, \partial_{tt}\mathbf{u} = \nabla\cdot\boldsymbol{\sigma} + \mathbf{F} & \text{on } \Omega\times[0,T], \\ \boldsymbol{u}(x,0) = u_0(x) & \text{for } x\in\Omega, \\ \partial_t\boldsymbol{u}(x,0) = v_0(x) & \text{for } x\in\Omega, \\ \boldsymbol{\sigma}\hat{\mathbf{n}} = 0 & \text{on } \partial\Omega \end{cases} \tag{72}$$

defined over $\Omega = [0,1]^3$ we keep the general definition

$$\sigma_{ij} = c_{ijkl}\varepsilon_{lk}, \qquad \varepsilon_{ij} = \frac{1}{2}\left(\partial_j u_i + \partial_i u_j\right) \tag{73}$$

of the Cauchy stress tensor $\boldsymbol{\sigma}$. The derivation follows similar lines as for the isotropic case. We start from decoupling the equations by introducing $\mathbf{v} = \partial_t\mathbf{u}$

$$\begin{cases} \partial_t\mathbf{u} = \mathbf{v}, \\ \rho\,\partial_t\mathbf{v} = \nabla\cdot\boldsymbol{\sigma} + \mathbf{F}. \end{cases} \tag{74}$$

Again, we split every time-step into three sub-steps

$$\begin{cases} \mathbf{u}^{(t+\frac{1}{3})} = \mathbf{u}^{(t)} + \dfrac{\tau}{3}\mathbf{v}^{(t)}, \\ \rho\mathbf{v}^{(t+\frac{1}{3})} = \rho\mathbf{v}^{(t)} + \dfrac{\tau}{3}\left(\nabla\cdot\boldsymbol{\sigma}^{(t+\frac{1}{3})} + \mathbf{F}\right), \end{cases} \tag{75}$$

$$\begin{cases} \mathbf{u}^{(t+\frac{2}{3})} = \mathbf{u}^{(t+\frac{1}{3})} + \dfrac{\tau}{3}\mathbf{v}^{(t+\frac{1}{3})}, \\ \rho\mathbf{v}^{(t+\frac{2}{3})} = \rho\mathbf{v}^{(t+\frac{1}{3})} + \dfrac{\tau}{3}\left(\nabla\cdot\boldsymbol{\sigma}^{(t+\frac{2}{3})} + \mathbf{F}\right), \end{cases} \tag{76}$$

$$\begin{cases} \mathbf{u}^{(t+1)} = \mathbf{u}^{(t+\frac{2}{3})} + \dfrac{\tau}{3}\mathbf{v}^{(t+\frac{2}{3})}, \\ \rho\mathbf{v}^{(t+1)} = \rho\mathbf{v}^{(t+\frac{2}{3})} + \dfrac{\tau}{3}\left(\nabla\cdot\boldsymbol{\sigma}^{(t+1)} + \mathbf{F}\right). \end{cases} \tag{77}$$

Here we follow the idea similar to the isotropic case, where $\boldsymbol{\sigma}^{(t+\frac{k}{3})}$ are constructed using

$$\mathbf{u} = \mathbf{u}^{(t+\frac{k-1}{3})} + \frac{\tau}{3}\mathbf{v}^{(t+\frac{k-1}{3})}$$

in most places, except when u_i appears inside i-th component of $\nabla\cdot\boldsymbol{\sigma}$ under a double derivative with respect to x ($k=1$), y ($k=2$) or z ($k=3$). After separating the operator into its diagonal part and its off-diagonal part, treating the diagonal part implicitly, and the rest explicitly, we obtain now the following form of the left-hand side (differences denoted in red color):

$$\begin{cases} \rho\, v_x^{(t+\frac{1}{3})} - \dfrac{\tau}{3} c_{1111}\,\partial_{xx} v_x^{(t+\frac{1}{3})} \\ \rho\, v_y^{(t+\frac{1}{3})} - \dfrac{\tau}{6}\left(c_{2121}+c_{2112}\right)\partial_{xx} v_y^{(t+\frac{1}{3})} \\ \rho\, v_z^{(t+\frac{1}{3})} - \dfrac{\tau}{6}\left(c_{3131}+c_{3113}\right)\partial_{xx} v_z^{(t+\frac{1}{3})} \end{cases} \tag{78}$$

$$\begin{cases} \rho\, v_x^{(t+\frac{2}{3})} - \dfrac{\tau}{6}\left(c_{1212}+c_{1221}\right)\partial_{yy} v_x^{(t+\frac{2}{3})} \\ \rho\, v_y^{(t+\frac{2}{3})} - \dfrac{\tau}{3} c_{2222}\,\partial_{yy} v_y^{(t+\frac{2}{3})} \\ \rho\, v_z^{(t+\frac{2}{3})} - \dfrac{\tau}{6}\left(c_{3232}+c_{3223}\right)\partial_{yy} v_z^{(t+\frac{2}{3})} \end{cases} \tag{79}$$

$$\begin{cases} \rho\, v_x^{(t+1)} - \dfrac{\tau}{6}\left(c_{1313}+c_{1331}\right)\partial_{zz} v_x^{(t+1)} \\ \rho\, v_y^{(t+1)} - \dfrac{\tau}{6}\left(c_{2323}+c_{2332}\right)\partial_{zz} v_y^{(t+1)} \\ \rho\, v_z^{(t+1)} - \dfrac{\tau}{3} c_{3333}\,\partial_{zz} v_z^{(t+1)} \end{cases} \tag{80}$$

The rest of the derivation is identical to the isotropic case. The stability analysis for the elastic wave propagation in isotropic and anisotropic cases is an open problem at this point.

8. CONCLUSIONS

This paper introduces mixed space-time discretizations based on the alternating direction method in space and the implicit time-stepping scheme. The intermediate time steps process the Kronecker product structure of the matrix to invert local matrices in linear $\mathcal{O}(N)$ computational cost. The resulting isogeometric implicit alternating direction method is conditionally stable, with $\Delta t \leq Cmin(h_x, h_y, h_z)$, where C is a problem and discretization dependent constant. The proposed splitting of the seismic P-wave and elastic wave propagation problems requires

introducing the three intermediate time steps to preserve the Kronecker product structure of the matrices. Summing up, we have reduced the computational cost of factorization with respect to the fully implicit schemes from $\mathcal{O}(N^2)$ [39] down to $\mathcal{O}(N)$ for a price of introducing intermediate time steps with the limitation of the time step size by the diameter of the element. We have implemented the seismic P-wave, and elastic wave propagation problems in the IGA-ADS library [29]. The code can be found at [29]. Future work may include generalization to other wave propagation problems [40, 41],

ACKNOWLEDGEMENTS

This work is supported by the European Union's Horizon 2020 Research and Innovation Program of the Marie Skłodowska-Curie grant agreement No. 777778 (MATHROCKs).

REFERENCES

[1] W. Lowrie, *The Fundamentals of Geophysics.* Cambridge University Press, 1997.

[2] C.M.R. Fowler, *The solid Earth: an introduction to global geophysics.* Cambridge University Press, 2005.

[3] D. Komatitsch, J. Ritsemaand, and J. Tromp, "The Spectral-Element Method, Beowulf Computing, and Global Seismology," *Science*, vol. 298, no. 5599, pp. 1737–1742, 2002.

[4] S.-J. Lee, C. How-Wei, Q. Liu, D. Komatitsch, B.-S. Huang, and J. Tromp, "Three-Dimensional Simulations of Seismic-Wave Propagation in the Taipei Basin with Realistic Topography Based upon the Spectral-Element Method," *Bull. Seismol. Soc. Am.*, vol. 98, no. 1, pp. 253–264, 2002.

[5] M. Gade, and S.T.G.Raghukanth, "Seismic ground motion in micropolar elastic half-space," *Appl. Math. Modell.*, vol. 39, no. 23–24, pp. 7244–7265, 2015.

[6] J.A. Cottrell, T.J.R. Hughes, and Y. Bazilevs, *Isogeometric Analysis: Toward Unification of CAD and FEA.* John Wiley and Sons, 2009.

[7] M.-C. Hsu, I. Akkerman, and Y. Bazilevs, "High-performance computing of wind turbine aerodynamics using isogeometric analysis," *Comput. Fluids*, vol. 49, no. 1, pp. 93–100, 2011.

[8] K. Chang, T.J.R. Hughes, and V.M. Calo, "Isogeometric variational multiscale large-eddy simulation of fully-developed turbulent flow over a wavy wall," *Comput. Fluids*, vol. 68, pp. 94–104, 2022.

[9] L. Dedè,T.J.R. Hughes, S. Lipton, and V.M. Calo, "Structural topology optimization with isogeometric analysis in a phase field approach," *USNCTAM2010, 16th US National Congree of Theoretical and Applied Mechanics*, 2010.

[10] L. Dedè, M. J. Borden, and T.J.R. Hughes, "Isogeometric analysis for topology optimization with a phase field model," ICES REPORT 11-29, The Institute for Computational Engineering and Sciences, The University of Texas at Austin, 2011.

[11] H. Gómez, V.M. Calo, Y. Bazilevs, and T.J.R. Hughes, "Isogeometric analysis of the Cahn-Hilliard phase-field model," *Comput. Meth. Appl. Mech. Eng.*, vol. 197, pp. 4333–4352, 2008.

[12] H. Gómez, T.J.R. Hughes, X. Nogueira, and V.M. Calo, "Isogeometric analysis of the isothermal Navier-Stokes-Korteweg equations," *Comput. Meth. Appl. Mech. Eng.*, vol. 199, pp. 1828–1840, 2010.

[13] R. Duddu, L. Lavier, T.J.R. Hughes, and V.M. Calo, "A finite strain Eulerian formulation for compressible and nearly incompressible hyper-elasticity using high-order NURBS elements," *Int. J. Numer. Meth. Eng.*, vol. 89, no. 6, pp. 762–785, 2012.

[14] S. Hossain, S.F.A. Hossainy, Y. Bazilevs, V.M. Calo, and T.J.R. Hughes, "Mathematical modeling of coupled drug and drug-encapsulated nanoparticle transport in patient-specific coronary artery walls," *Comput. Mech.*, vol. 49, pp. 213–242, 2011.

[15] Y. Bazilevs, V.M. Calo, Y. Zhang, and T.J.R. Hughes: "Isogeometric fluid-structure interaction analysis with applications to arterial blood flow," *Comput. Mech.*, vol. 38, pp. 310–322, 2006.

[16] Y. Bazilevs, V.M. Calo, J.A. Cottrell, T.J.R. Hughes, A. Reali, and G. Scovazzi, "Variational multiscale residual-based turbulence modeling for large eddy simulation of incompressible flows," *Comput. Meth. Appl. Mech. Eng.*, vol. 197, pp. 173–201, 2007.

[17] V.M. Calo, N. Brasher, Y. Bazilevs, and T.J.R. Hughes, "Multiphysics Model for Blood Flow and Drug Transport with Application to Patient-Specific Coronary Artery Flow," *Comput. Mech.*, vol. 43, no. 1, pp. 161–177, 2008.

[18] M. Łoś, M. Paszyński, A. Kłusek, and W. Dzwinel, "Application of fast isogeometric L2 projection solver for tumor growth simulations," *Comput. Meth. Appl. Mech. Eng.*, vol. 316, pp. 1257–1269, 2017.

[19] M. Łoś, A. Kłusek, M. Amber Hassam, K. Pingali, W. Dzwinel, and M. Paszyński, "Parallel fast isogeometric L2 projection solver with GALOIS system for 3D tumor growth simulations," *Comput. Meth. Appl. Mech. Eng.*, vol. 343, pp. 1–22, 2019.

[20] M. Łoś, M. Woźniak, I. Muga, and M. Paszyński, "Three-dimensional simulations of the airborne COVID-19 pathogens using the advection-diffusion model and alternating-directions implicit solver," *Bull. Pol. Acad. Sci. Tech. Sci.*, vol. 69, no. 4, pp. 1–8, 2021.

[21] Y. Bazilevs, L. Beirao da Veiga, J.A. Cottrell, T.J.R. Hughes, and G. Sangalli, "Isogeometric Analysis: Approximation, stability and error estimates for h-refined meshes," *Math. Models Meth. Appl. Sci.*, vol. 16, no. 7, pp. 1031–1090, 2006.

[22] D.W. Peaceman and H.H. Rachford Jr., "The numerical solution of parabolic and elliptic differential equations," *J. Soc. Ind. Appl. Math.*, vol. 3, pp. 28-–41, 1955.

[23] J.L. Guermond and P. Minev, "A new class of fractional step techniques for the incompressible Navier-Stokes equations using direction splitting," *C. R. Math.*, vol. 348, no. 9–10, pp. 581-–585, 2010.

[24] J.L. Guermond, P. Minev, and J. Shen, "An overview of projection methods for incompressible flows," *Comput. Meth. Appl. Mech. Eng.*, vol. 195, pp. 6011—6054, 2006.

[25] L. Gao and V.M. Calo, "Fast isogeometric solvers for explicit dynamics," *Comput. Meth. Appl. Mech. Eng.*, vol. 274, no. 1, pp. 19–41, 2014.

[26] L. Gao and V.M. Calo, "Preconditioners based on the alternating-direction-implicit algorithm for the 2D steady-state diffusion equation with orthotropic heterogeneous coefficients," *J. Comput. Appl. Math.*, vol. 273, no. 1, pp. 274–295, 2015.

[27] L. Gao, *Kronecker products on preconditioning.* PhD. Thesis, King Abdullah University of Science and Technology, 2013.

[28] G. Gurgul and M. Paszyński, "Object-oriented implementation of the Alternating Directions Implicit Solver for Isogeometric Analysis," *Adv. Eng. Software*, vol. 128, pp. 187–220, 2019.

[29] M. Łoś, M. Woźniak, M. Paszyński, A. Lenharth, and K. Pingali, "IGA-ADS: Isogeometric Analysis FEM using ADS solver," *Comput. Phys. Commun.*, vol. 217, pp. 99–116, 2017. https://github.com/marcinlos/iga-ads.

[30] M. Łoś and M. Paszyński, "Applications of Alternating Direction Solver for simulations of time-dependent problems," *Comput. Sci.*, vol. 18, no. 2, pp. 117–128, 2017.

[31] R.I. Fernandes and G. Fairweather, "An Alternating Direction Galerkin Method for a Class of Second-Order Hyperbolic Equations in Two Space Variables," *SIAM J. Numer. Anal.*, vol. 28, no.5, pp. 1265–1281, 1991.

[32] H. Lim, S. Kim, and J. Douglas Jr., "Numerical methods for viscous and nonviscous wave equations," *Appl. Numer. Math.*, vol. 57, no. 2, pp. 194–212, 2007.

[33] G. Gurgul, M. Łoś, and M. Paszyński, "Linear computational cost implicit solver for parabolic problems," *Comput. Sci.*, vol. 21, no. 3, pp. 335–352, 2020.

[34] M. Paszyński, "Convergence of iterative solvers for non-linear Step-and-Flash Imprint Lithography Simulations," *Comput. Sci.*, vol. 12, pp. 63–83, 2011.

[35] M. Paszyński, T. Jurczyk, and D. Pardo, "Multi-frontal solver for simulations of linear elasticity coupled with acoustics," *Comput. Sci.*, vol. 12, pp. 85–102, 2011.

[36] M. Łoś, P. Behnoudfar, M. Paszyński, and V. Calo, "Fast isogeometric solvers for hyperbolic wave propagation problems," *Comput. Math. Appl.*, vol. 80, no. 1, pp. 109–120, 2020.

[37] N.M. Newmark, "A method of computation for structural dynamics," *J. Eng. Mech.*, vol. 85 (EM3), pp. 67–94, 1959.

[38] A. Graham, *Kronecker products, matrix calculus with applications*, Dover, 2018.

[39] M. Paszyński, *Fast solvers for mesh-based computations.* Taylor & Francis, CRC Press, 2016.

[40] T. Kapitaniak, M. Sofer, B. Błachowski, W. Sochacki, and S. Garus, "Vibrations, mechanical waves, and propagation of heat in physical systems," *Bull. Pol. Acad. Sci. Tech. Sci.*, vol. 70, p. e140149, 2022.

[41] S. Garus, W. Sochacki, M. Kubanek, and M. Nabiałek, "Minimizing the number of layers of the quasi one-dimensional phononic structures," *Bull. Pol. Acad. Sci. Tech. Sci.*, vol. 70, p. e139394, 2022.